

## Electronic Supplementary Information

### Unique catalytic property of Ni-Ir alloy for hydrogenation of *N*-heteroaromatics

Jia-qi Bai,<sup>a,b</sup> Masazumi Tamura,<sup>c,\*</sup> Yoshinao Nakagawa,<sup>a</sup> Keiichi Tomishige<sup>a,\*</sup>

<sup>a</sup>Department of Applied Chemistry, School of Engineering, Tohoku University, 6-6-07, Aoba, Aramaki, Aoba-ku, Sendai 980-8579, Japan

<sup>b</sup>School of Chemistry and Chemical Engineering, Anhui University, Hefei 230061, China.

<sup>c</sup>Research Center for Artificial Photosynthesis, Osaka City University, 3-3-138, Sugimoto, Sumiyoshi-ku, Osaka, 558-8585, Japan.

Email: [mtamura@osaka-cu.ac.jp](mailto:mtamura@osaka-cu.ac.jp), [tomi@erec.che.tohoku.ac.jp](mailto:tomi@erec.che.tohoku.ac.jp)

## Experimental

### 1.1 General

The products were analyzed by GC (Shimadzu GC-2014) and GC-MS (Shimadzu QP-5050) with DB-1 capillary column (GL Sciences Inc., diameter 0.25 mm, 30 m) for hydrogenation of pyridines. All chemicals were purchased from commercial chemical companies and used without further purification. Pyridine (Sigma-Aldrich, >99.8%), piperidines (FUJIFILM Wako Pure Chemical Corporation, >99%), 2-methylpyridine (FUJIFILM Wako Pure Chemical Corporation, >98%), pyrazine (Sigma-Aldrich, >99%), quinoline (FUJIFILM Wako Pure Chemical Corporation, >95%), isoquinoline (Tokyo Chemical Industry Co., Ltd. >98%), indole (Tokyo Chemical Industry Co., Ltd., >99%), methanol (Kanto Chemical Co., Inc. >99.8%), *n*-dodecane (Tokyo Chemical Industry Co., Ltd., >99%), ethanol (Kanto Chemical Co., Inc. >99.5%).

### 1.2 Catalyst preparation

Ni-Ir/SiO<sub>2</sub> was prepared by sequential impregnation method [S1]. Ir/SiO<sub>2</sub> was synthesized by impregnating SiO<sub>2</sub> (Fuji Silysia Ltd., G-6, calcined at 973 K, 1 h) with H<sub>2</sub>IrCl<sub>6</sub> aqueous solution (Furuya Metals Co., Ltd.), and then it was dried in oven at 373 K overnight after removal of water by evaporation on a hotplate at 353 K. Ni was loaded on the Ir/SiO<sub>2</sub> by impregnating Ir/SiO<sub>2</sub> with Ni(NO<sub>3</sub>)<sub>2</sub> (Wako Pure Chemical Industries, Ltd.) aqueous solution, followed by drying in oven at 373 K overnight after removal of water by evaporation on a hotplate at 353 K. Finally, the obtained dried Ni-Ir/SiO<sub>2</sub> was calcined at 773 K for 3 h in muffle furnace. Ni-Ir/SiO<sub>2</sub> was reduced under H<sub>2</sub> flow (30 ml/min) at 773 K for 1 h just before use, and obtained catalysts were described as Ni-Ir/SiO<sub>2</sub>-X(*T*), where X is the introduced Ni/Ir molar ratio and *T* is the reduction temperature (if not described, *T* is 773 K). M-Ir/SiO<sub>2</sub> (Ir 4wt%, M=Co, Fe and Cu, M/Ir=1) and Ni-M'/SiO<sub>2</sub> ((M'=Pd, Ru and Pt, M 4 wt%, Ni/M=1) were prepared by the same method as described above for the synthesis of Ni-Ir/SiO<sub>2</sub> [S2], but using different precursors. The used precursors and supports are Co(NO<sub>3</sub>)<sub>2</sub>·6H<sub>2</sub>O (Wako

Pure Chemical Industries, Ltd.),  $\text{Fe}(\text{NO}_3)_3 \cdot 9\text{H}_2\text{O}$  (Wako Pure Chemical Industries, Ltd.)  $\text{Cu}(\text{NO}_3)_2 \cdot 3\text{H}_2\text{O}$  (Wako Pure Chemical Industries, Ltd.),  $\text{Pd}(\text{NO}_3)_2$ aq (Ne. Chemcat. Corporation),  $\text{Ru}(\text{NO})(\text{NO}_3)_3$  (Strem Chemicals, Inc) and  $\text{Pt}(\text{NH}_3)_4(\text{NO}_3)_2$  (Sigma-Aldrich Corporation), respectively.

### 1.3 Typical procedure for hydrogenation of pyridine

Activity tests were conducted in a 190-ml stainless steel autoclave with an inserted glass vessel. The standard reaction conditions for hydrogenation of pyridine are as follows: the reduced catalyst (typically 20 mg), a spinner and mixture of pyridine (5 mmol) and methanol (3 g) were added into the glass vessel in the autoclave under air except for Ni/SiO<sub>2</sub>. Ni/SiO<sub>2</sub> catalyst was transferred into the autoclave in glovebox with N<sub>2</sub> in order to avoid oxidation of Ni metal species by exposing it to air. The air was purged by flushing with H<sub>2</sub> (1 MPa, 99.99%, Nippon Peroxide Co., Ltd.) three times after sealing the reactor and the pressure was raised to 1 MPa by H<sub>2</sub> at room temperature. Then, the autoclave was heated to 353 K and H<sub>2</sub> pressure was increased to 8 MPa and the stirring speed was fixed at 500 rpm. The reaction temperature was monitored by a thermocouple inserted in the autoclave. After the reaction, the reactor was cooled to room temperature in water bath. The liquid phase was transferred to a vial and then washed by 10 g ethanol. The products were analyzed by GC with DB-1 capillary column. Conversion of the pyridine and selectivity of products were calculated by GC with *n*-dodecane (about 0.2 g) as an internal standard. TOF and TOF<sub>s</sub> was calculated as follows:  $\text{TOF} (\text{min}^{-1}) = (\text{Produced piperidine amount (mmol)})/(\text{total Ir and Ni metal amount (mmol)})/(\text{Time (min)})$ ,  $\text{TOF}_s (\text{min}^{-1}) = (\text{Produced piperidine amount (mmol)})/(\text{surface metal amount (mmol)})/(\text{Time (min)})$ . The surface metal amount (mmol) was calculated by integration of total metal amount with dispersion determined by H<sub>2</sub> adsorption. The qualitative analysis was conducted by GC-MS with DB-1 capillary column.

As for the reusability test, the catalyst was recovered from the reaction mixture by centrifugation. After washing with ethanol (20 g) and drying, the catalyst was calcined at 723

K in air for 1 h and reduced at 773 K for 1 h (c) for the next reaction under the same reaction conditions as the activity test.

The amount of isolated Ni amount is calculated on the basis of following assumptions, and the equation is shown in eq. 1.

1. All Ir metals are used for alloy formation.
2. Alloy surface is fcc (111).
3. Composition of Ni-Ir alloys is based on the results of XRD by using Vegard's law.
4. Ni-Ir Alloys are well-mixed ones.

Amount of isolated Ni amount ( $\text{mmol g}^{-1}$ ) = (Surface Ni in Ni-Ir alloy ( $\text{mmol g}^{-1}$ ))  $\times$   $(1 - \text{Ni}/(\text{Ni} + \text{Ir}))^6$  ..... (eq. 1)

$\text{Ni}/(\text{Ni} + \text{Ir})$  is the alloy composition in the Ni-Ir alloy of Ni-Ir/SiO<sub>2</sub> catalysts.  $(1 - \text{Ni}/(\text{Ni} + \text{Ir}))$  represents the probability of the absence of Ni species around one Ni site, and the superscript 6 after  $(1 - \text{Ni}/(\text{Ni} + \text{Ir}))$  represents the number of metal sites around one certain Ni site.

Surface Ni in Ni-Ir alloy ( $\text{mmol g}^{-1}$ ) was calculated by assuming that the dispersion is 20% in Ni-Ir alloys as shown in eq. 2

Surface Ni in Ni-Ir alloy ( $\text{mmol g}^{-1}$ ) = Ir amount ( $\text{mmol g}^{-1}$ )  $\times A/(1 - A) \times 0.2$  .... (eq. 2)

A is the alloy composition of Ni/(Ir+Ni) in Table S3.

## 1.4 Characterization

X-ray diffraction (XRD) patterns were recorded by a diffractometer (MiniFlex600, Rigaku). Cu K $\alpha$  ( $\lambda = 0.154$  nm, 45 kV, 40 mA) radiation was used as an X-ray source. In order to precisely obtain the position of XRD peaks, the sample was mixed with Si powder (Wako Pure Chemical Industries, Ltd. 99.9%) for measurement and XRD patterns were calibrated by Si (111) of 28.42°. The average metal particle size was estimated using Scherrer's equation.

The amount of leached metals (Ir and Ni) into the reaction solution was analyzed by inductively coupled plasma atomic emission spectroscopy (ICP-AES, Thermo Fisher

Scientific iCAP 6500).

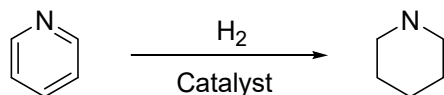
The amount of H<sub>2</sub> adsorption was measured in a high-vacuum system using a volumetric method. The catalyst (~0.1 g) in the measurement cell was reduced with H<sub>2</sub> at 773 K for 1 h and evacuated at 773 K for 1 h. After cooling, the adsorption amount of H<sub>2</sub> was measured at room temperature. Gas pressure at adsorption equilibrium was about 1.1 kPa. The dead volume of the apparatus was 36.26 cm<sup>3</sup>. H<sub>total</sub> was calculated based on the H atom amount of total adsorbed H<sub>2</sub> amount (sum of physical and chemical adsorption).

X-ray absorption spectroscopy (XAS) was conducted at the BL01B1 station at SPring-8 with the approval of the Japan Synchrotron Radiation Research Institute (JASRI; Proposal No. 2018B1805). The storage ring was operated at 8 GeV, and a Si (111) single crystal was used to obtain a monochromatic X-ray beam. Two ion chambers for I<sub>0</sub> and I were filled with 85% N<sub>2</sub>+15% Ar and 50% N<sub>2</sub>+50% Ar, respectively, for Ir L<sub>3</sub>-edge measurement. Two ion chambers for I<sub>0</sub> and I were filled with 100% N<sub>2</sub> and 15% N<sub>2</sub>+85% Ar, respectively, for Ni K-edge measurement. The sample after the reduction and reaction were used for measurement. The calcined Ni-Ir/SiO<sub>2</sub>-1 (152.6 mg) was pressed into self-supporting disk with 10 mm diameter and reduced at 773 K for 1 h under H<sub>2</sub> for the sample after reduction, and then it was transferred to a measurement cell using a glove box filled with N<sub>2</sub>. The catalytic reaction was conducted in the autoclave under the same reaction conditions as the standard reaction conditions for the sample after reaction, and, the autoclave was also transferred to glove box and the catalyst was transferred to a measurement cell after drying with thickness of 2 mm. The thickness of the cell filled with the powder was adjusted to give an edge jump of 0.2–1 for Ir L<sub>3</sub>-edge and Ni K-edge measurement. The EXAFS data was collected by transmission mode for Ir L<sub>3</sub>-edge and fluorescence mode for Ni K-edge. For EXAFS analysis, the oscillation was first extracted from the EXAFS data using a spline smoothing method [S3]. Fourier transformation of the k<sup>3</sup>-weighted EXAFS oscillation from the k space to the r space was performed to obtain a radial distribution function. The inversely Fourier filtered data were analyzed using a usual curve fitting method [S4,5]. For curve fitting analysis, the empirical

phase shift and amplitude function for the Ir-Ir bond and Ni-Ni bond were extracted from the data for Ir powder and Ni foil. Theoretical functions for Ir-Ni bond and Ni-Ir bond were calculated by the FEFF8.2 program [S6]. Analyses of EXAFS and XANES data were performed using a computer program (REX2000, ver. 2.6.0; Rigaku Corporation).

## Supplementary Figures and Tables

**Table S1** Summary for the reports on heterogeneous catalysts for hydrogenation of pyridine

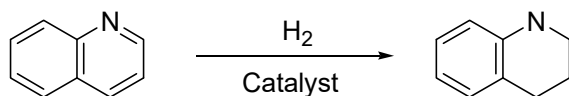


Catalyst	Solvent	$P_{H_2}$ [MPa]	$T$ [K]	$t$ [h]	Conv. [%]	Sel. [%]	Yield [%]	TOF <sup>a</sup> [h <sup>-1</sup> ]	TOF <sub>s</sub> <sup>b</sup> [h <sup>-1</sup> ]	Ref.
Rh colloidal	H <sub>2</sub> O	0.1	293	7	-	-	100	85	-	[S7]
Ru/PVPy	THF	5	423	-	-	>99	-	101	-	[S8]
Ru/MgO	THF	5	423	-	-	-	-	1232	4400	[S9]
Rh/MgO	Neat	1	423	-	-	>99	-	1338	44600	[S10]
Rh NPs supported in IL(ionic liquid) NHC(N-heterocyclic carbenes)- stabilized Rh nanoparticles	Neat	3	353	15	-	-	90	6	-	[S11]
Co/Melamine-6@TiO <sub>2</sub> -800-5	Methanol	2	303	2	100	>99	-	-	305	[S12]
Ti <sub>3</sub> -BPDC(biphenyl-4,4'-dicarboxylate)- CoH	Octane	6	433	24	-	-	99	0.5	-	[S13]
Co-pyromellitic acid@SiO <sub>2</sub> -800	2- Propanol/H <sub>2</sub> O =2/1	2	373	22	-	-	94	21	-	[S14]
Pd/C	AcOH	5	408	48	-	-	94	0.3	-	[S15]
Ru-PAL(2- (hexadecylaminomethyl)pyridine)-800	2-Propanol	0.1	298	15	-	-	100	0.7	-	[S16]
Pd/MgO-F	CH <sub>3</sub> OH	1	353	12	-	-	99	17	-	[S17]
Aluminum metal-organic framework-DUT- 5-CoH	<i>n</i> -Heptane	2	363	48	-	-	69	1.1	-	[S18]
Ni-Ir/SiO <sub>2</sub> -1	Methanol	3	423	6	-	-	80	33	-	[S19]
	Methanol	8	353	4	15	>99	15	22	230	This
	Methanol	8	353	8	99	>99	99	15	240	work

<sup>a</sup>The turnover frequency (TOF) per total metal amount.

<sup>b</sup>TOF per the surface metal (TOF<sub>s</sub>)

**Table S2** Summary for the reports on effective heterogeneous catalysts (TOF>100 h<sup>-1</sup>) and Ni-based catalysts for hydrogenation of quinoline



Catalyst	Solvent	$P_{H_2}$ [MPa]	$T$ [K]	$t$ [h]	Conv. [%]	Sel. [%]	Yield [%]	TOF <sup>a</sup> [h <sup>-1</sup> ]	TOF <sub>s</sub> <sup>b</sup> [h <sup>-1</sup> ]	Ref.
<i>Effective heterogeneous catalysts (TOF&gt;100 h<sup>-1</sup>)</i>										
Rh/Al <sub>2</sub> O <sub>3</sub>	IPA	2	373	2.5	100	99	98	231	-	[S20]
Pd-BT(black wattle tannin)-CF(collagen fiber)	H <sub>2</sub> O	2	333	1	99	>99	99	166	-	[S21]
Ru/PVPy(poly(4-vinylpyridine))	THF	5	423	-	-	29	-	171	-	[S8]
Au/HAS-TiO <sub>2</sub>	Toluene	2	314	48	100	-	97	101	-	[S22]
Pd/MgO	Neat	4	423	-	-	-	-	300	6400	[S23]
Ru/MgO	THF	5	423	-	-	-	-	952	3400	[S9]
Rh/MgO	Neat	4	423	-	-	>99	-	555	18500	[S10]
NHC(N-heterocyclic carbenes)-stabilized Rh nanoparticles	Neat	2	333	0.5	100	75	-	-	496	[S12]
Pt nanocatalyst	1-Pentanol + water	3	353	3	48	>99	-	160	-	[S24]
<i>Ni-based heterogeneous catalysts</i>										
Quenched skeletal Ni	THF	1.5	373	1.5	99	>99	99	1.8	-	[S25]
Nickel Nanoparticles	Ethanol	3	348	10	>99	99	99	12	29	[S26]
Raney Ni	Ethanol	3	348	10	83	90	75	6	-	[S26]
Ni-Co bimetallic nanoparticles	Ethanol	5	353	13	-	-	50	1.6	-	[S27]
Ni-Ir/SiO <sub>2</sub> -1	Methanol	8	353	4	37	98	36	56	573	This work

<sup>a</sup>The turnover frequency (TOF) per total metal amount.

<sup>b</sup>TOF per the surface metal (TOF<sub>s</sub>)

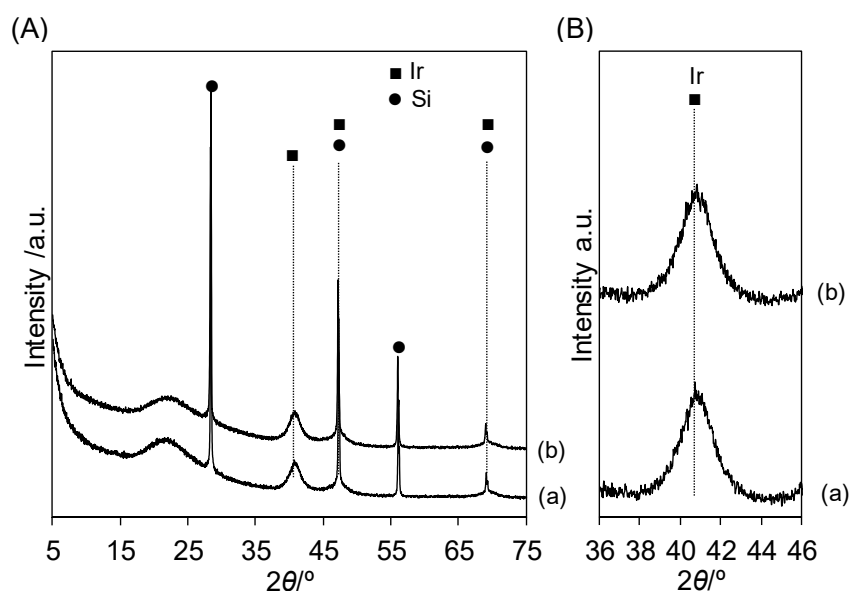


**Figure S1** XRD patterns of Ni-Ir/SiO<sub>2</sub>-0.15 and Ni-Ir/SiO<sub>2</sub>-0.2 catalysts after reduction (A) and the expanded figure (B)  
 (a) Ni-Ir/SiO<sub>2</sub>-0.15, (b) Ni-Ir/SiO<sub>2</sub>-0.2.  
 Si is the internal standard.

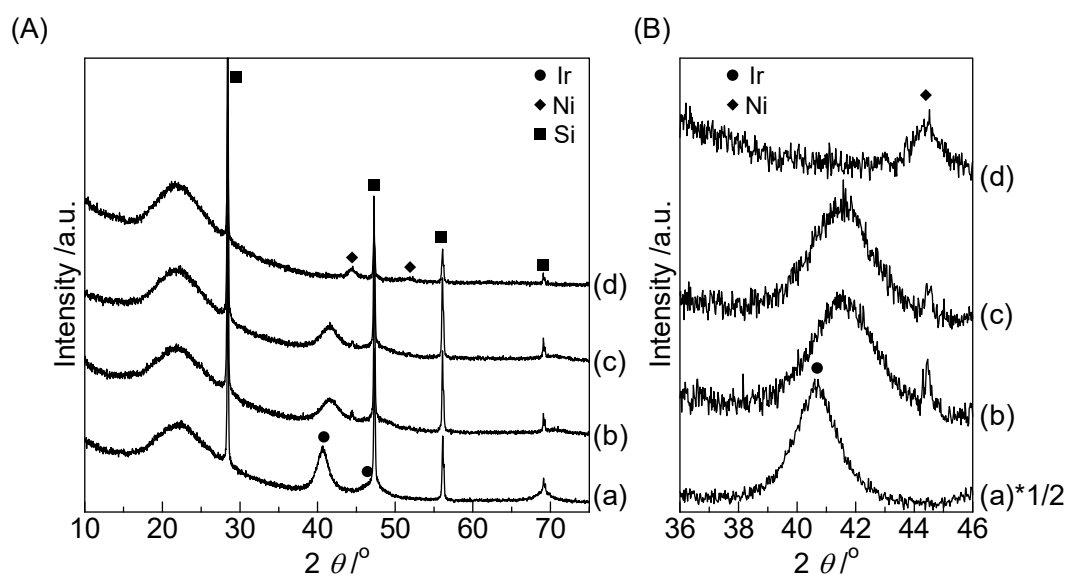


**Figure S2** XRD analyses. (A) XRD patterns of Ir/SiO<sub>2</sub>, Ni/SiO<sub>2</sub> and Ni-Ir/SiO<sub>2</sub>-1 after reduction and after reaction. (B) Expanded figure of (A).

(a) Ir/SiO<sub>2</sub> (Ir: 4 wt%) after reduction, (b) Ni-Ir/SiO<sub>2</sub>-1 after reduction, (c) Ni-Ir/SiO<sub>2</sub>-1 after reaction, (d) Ni/SiO<sub>2</sub> (Ni: 1.2 wt%) after reduction

Si is the internal standard.

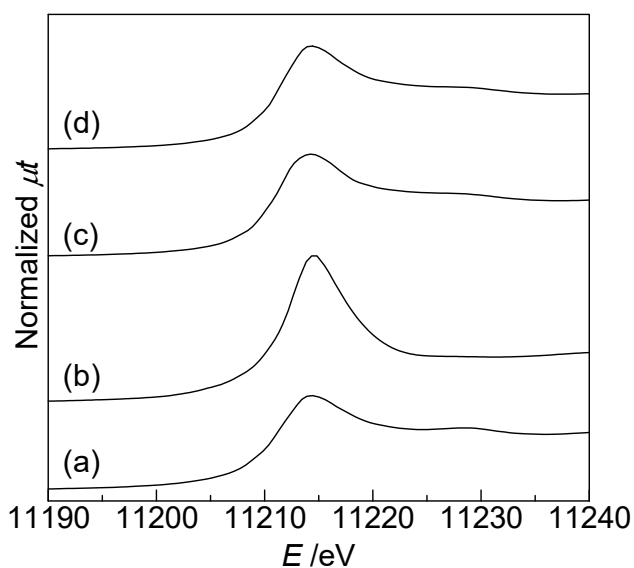


**Figure S3** Ir  $L_3$ -edge XANES spectra of Ni-Ir/SiO<sub>2</sub>-1 catalysts and related compounds. (a) Ir powder, (b) IrO<sub>2</sub>, (c) Ni-Ir/SiO<sub>2</sub>-1 after reduction<sup>a</sup>, (d) Ni-Ir/SiO<sub>2</sub>-1 after reaction. <sup>a</sup>The data is taken from [S1].

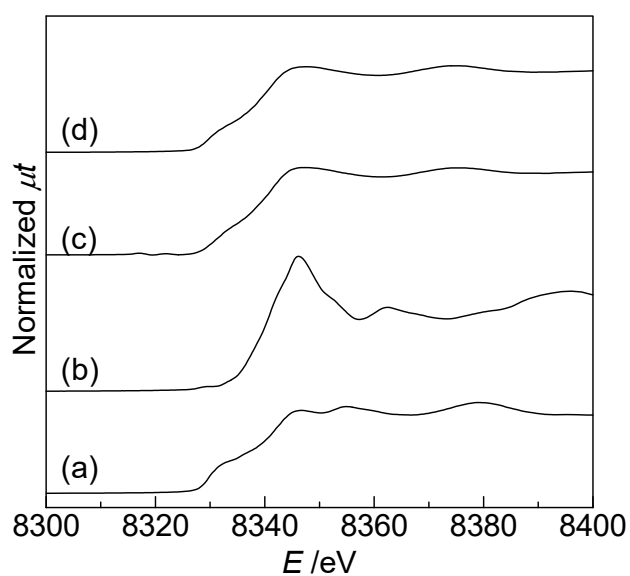


**Figure S4** Ni  $K$ -edge XANES spectra of Ni-Ir/SiO<sub>2</sub>-1 catalysts and related compounds. (a) Ni foil, (b) NiO, (c) Ni-Ir/SiO<sub>2</sub>-1 after reduction<sup>a</sup>, (d) Ni-Ir/SiO<sub>2</sub>-1 after reaction. <sup>a</sup>The data is taken from [S1].

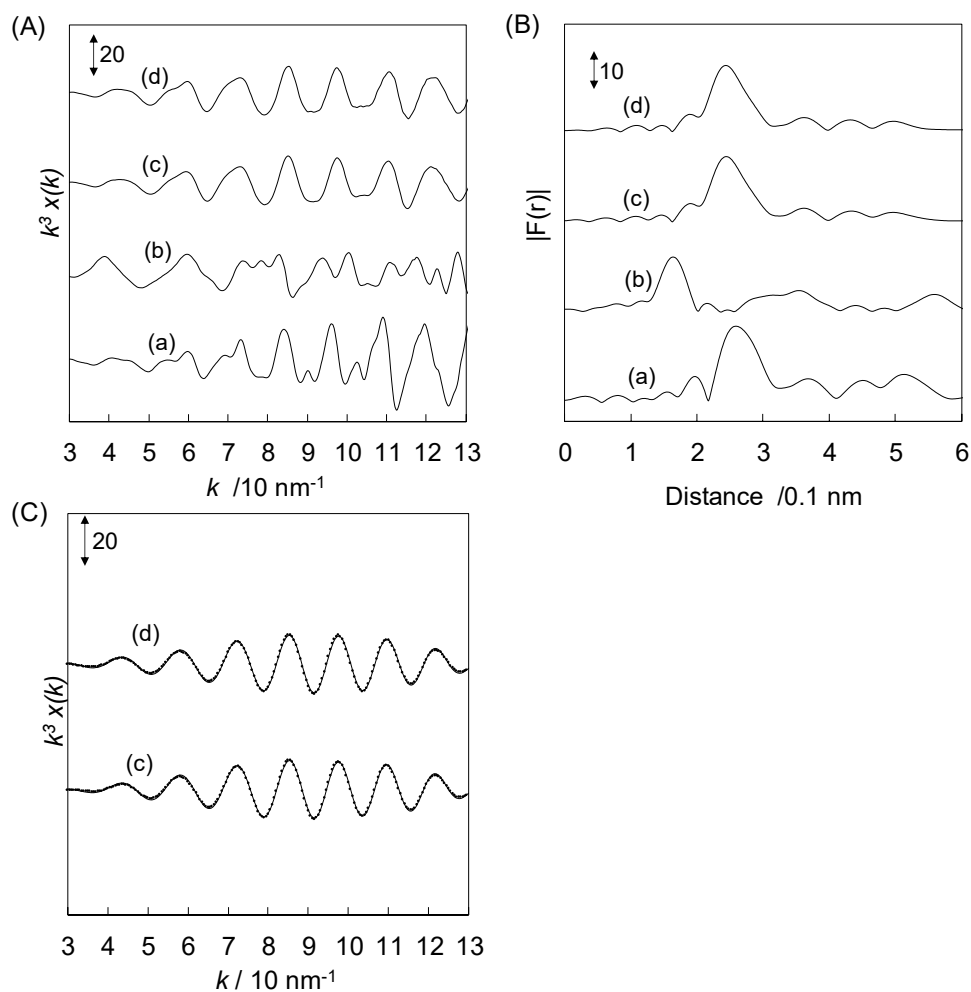


**Figure S5** Results of Ir  $L_3$ -edge EXAFS analyses of various Ir samples. (A)  $k^3$ -weighted Ir  $L_3$ -edge EXAFS oscillations, (B) Fourier transform of  $k^3$ -weighted Ir  $L_3$ -edge EXAFS, FT range 30-130  $\text{nm}^{-1}$ , (C) Fourier filtered Ni  $K$ -edge EXAFS data (solid line) and calculated data (dotted line). Fourier filtering range: 0.168-0.322 nm.

(a) Ir powder, (b)  $\text{IrO}_2$ , (c) Ni-Ir/ $\text{SiO}_2$ -1 after reduction <sup>a</sup>, (d) Ni-Ir/ $\text{SiO}_2$ -1 after reaction.

<sup>a</sup>The data are taken from [S1].

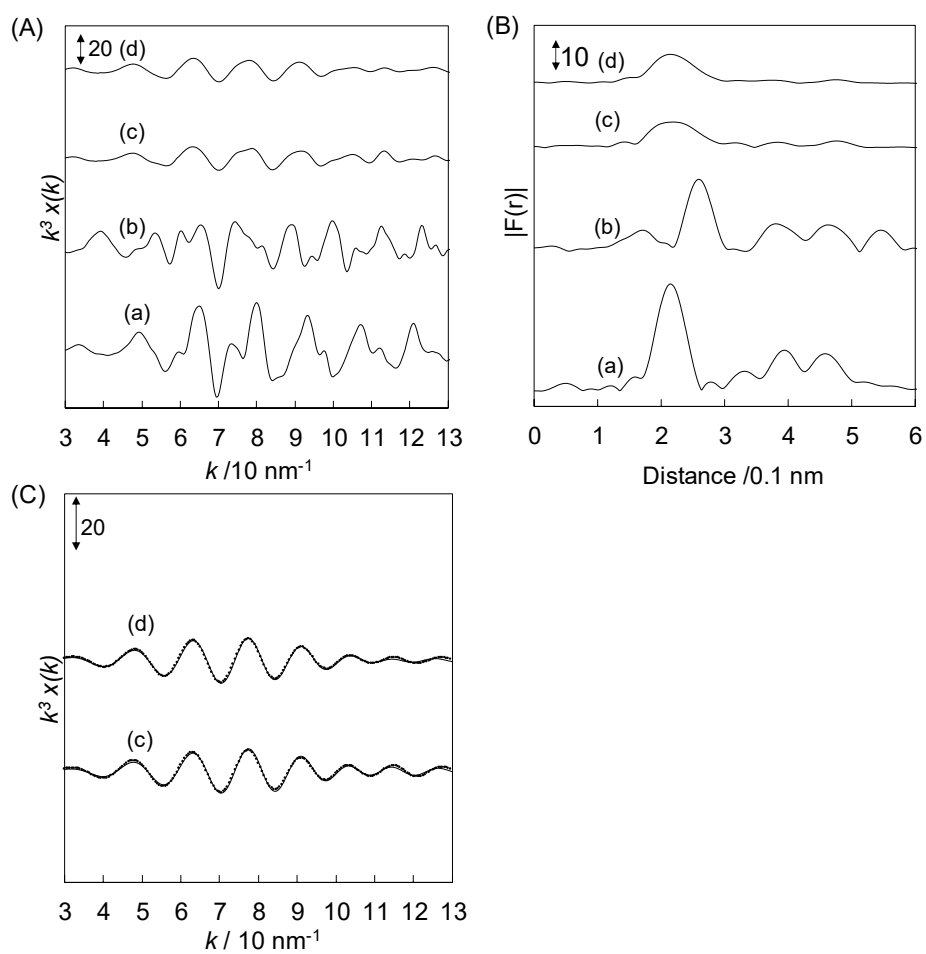


**Figure S6** Results of Ni *K*-edge EXAFS analyses of various Ni samples. (A)  $k^3$ -weighted Ni *K*-edge EXAFS oscillations. (B) Fourier transform of  $k^3$ -weighted Ni *K*-edge EXAFS, FT range 30-130  $\text{nm}^{-1}$ . (C) Fourier filtered Ni *K*-edge EXAFS data (solid line) and calculated data (dotted line). Fourier filtering range: 0.150-0.298 nm.

(a) Ni foil, (b) NiO, (c) Ni-Ir/SiO<sub>2</sub>-1 after reduction <sup>a</sup>, (d) Ni-Ir/SiO<sub>2</sub>-1 after reaction.

<sup>a</sup>The data are taken from [S1].

**Table S3** Curve fitting results of Ir  $L_3$ -edge EXAFS of Ni-Ir/SiO<sub>2</sub>-1 after reduction and after reaction

Catalyst	Condition	Shells	CN <sup>a</sup>	$R^b / 10^{-1}$ nm	$\sigma^c / 10^{-1}$ nm	$\Delta E_0^d /$ eV	$R_f^e / \%$
Ni-Ir/SiO <sub>2</sub> -1 <sup>f</sup>	after reduction	Ir-Ir	8.9	2.73	0.064	-3.6	0.3
		Ir-Ni	2.4	2.59	0.066	9.9	
Ni-Ir/SiO <sub>2</sub> -1	after reaction	Ir-Ir	8.9	2.73	0.070	-2.2	0.3
		Ir-Ni	2.4	2.60	0.067	10.0	
Ir powder	–	Ir-Ir	12	2.77	0.060	0	–

<sup>a</sup>Coordination number. <sup>b</sup>Bond distance. <sup>c</sup>Debye-Waller factor. <sup>d</sup>Difference in the origin of photoelectron energy between the reference and the sample. <sup>e</sup>Residual factor. Fourier filtering range: 0.168–0.322 nm.

<sup>f</sup>The data are taken from [S1].

**Table S4** Curve fitting results of Ni  $K$ -edge EXAFS of Ni-Ir/SiO<sub>2</sub>-1 after reduction and after reaction

Catalyst	Condition	Shells	CN <sup>a</sup>	$R^b / 10^{-1}$ nm	$\sigma^c / 10^{-1}$ nm	$\Delta E_0^d /$ eV	$R_f^e / \%$
Ni-Ir/SiO <sub>2</sub> -1 <sup>f</sup>	after reduction	Ni-Ni	5.8	2.50	0.099	-7.8	1.6
		Ni-Ir	2.4	2.60	0.071	0.5	
Ni-Ir/SiO <sub>2</sub> -1	after reaction	Ni-Ni	5.8	2.51	0.094	-2.7	0.8
		Ni-Ir	2.4	2.60	0.077	-2.6	
Ni foil		Ni-Ni	12	2.49	0.06	0	–

<sup>a</sup>Coordination number. <sup>b</sup>Bond distance. <sup>c</sup>Debye-Waller factor. <sup>d</sup>Difference in the origin of photoelectron energy between the reference and the sample. <sup>e</sup>Residual factor. Fourier filtering range: 0.150–0.298 nm.

<sup>f</sup>The data are taken from [S1].

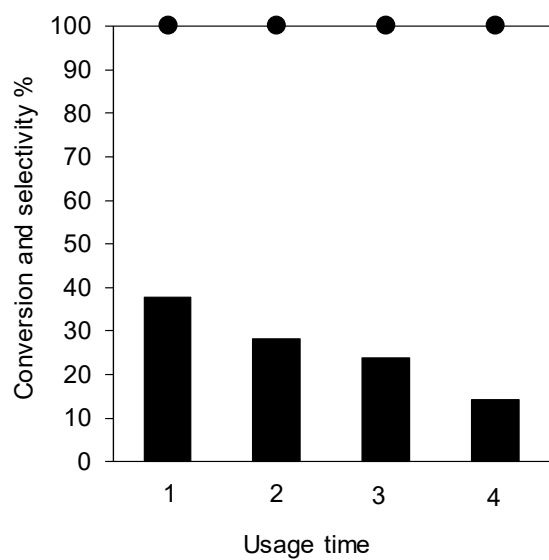


**Figure S7** Reusability test of Ni-Ir/SiO<sub>2</sub>-1 catalyst in hydrogenation of pyridine to piperidine.

Black bar: conversion. ●: selectivity to piperidine.

Reaction conditions: Ni-Ir/SiO<sub>2</sub>-1 0.1 g, pyridine 5 mmol, methanol 3 g, H<sub>2</sub> 8 MPa, 353 K, 2 h.

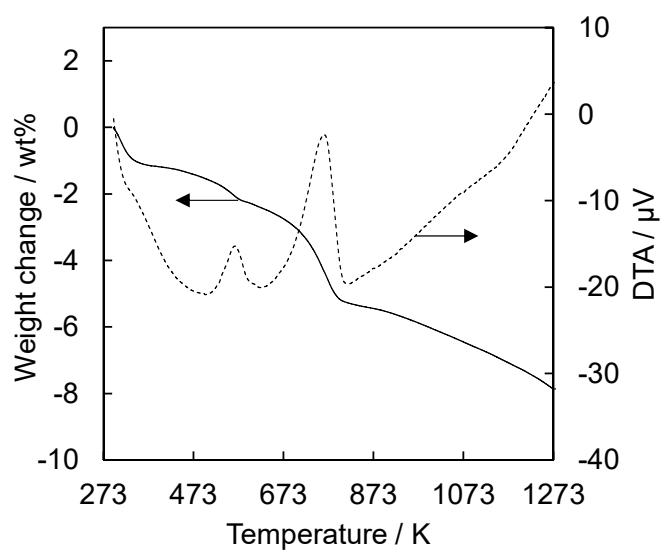


**Figure S8** TG-DTA analysis of the Ni-Ir/SiO<sub>2</sub>-1 after 1st use.

Heating rate = 10 K/min, sample weight = 10 mg.

Reaction conditions: pyridine 5 mmol, methanol 3 g, H<sub>2</sub> 8 MPa, 353 K, 2 h.

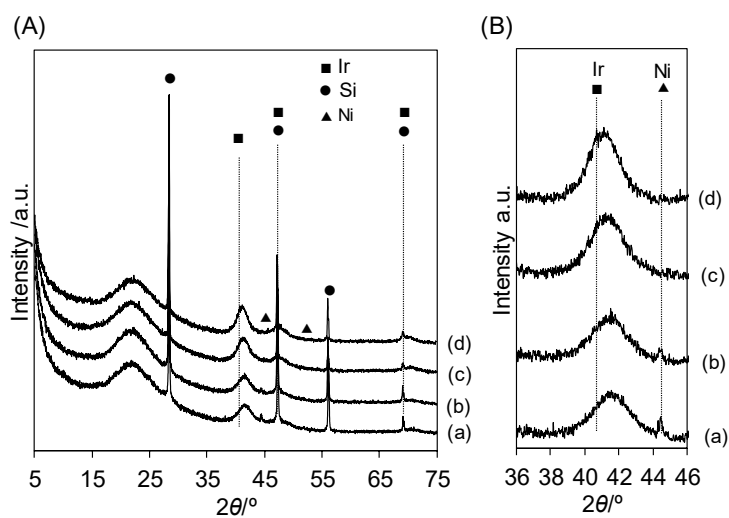


**Figure S9** XRD patterns of Ni-Ir/SiO<sub>2</sub>-1 catalysts after reduction and reuse (a) reduction, (b) after first run, (c) after second run and (d) after fourth run. (A) Full range signals and (B) expanded signals at the range from 36 to 46°.

Si is the internal standard.

**Table S5** Summary of the alloy compositions and particle sizes of fresh and used Ni-Ir/SiO<sub>2</sub>-1 catalysts<sup>a</sup>

Usage time	Catalyst pretreatment conditions before XRD measurement	Alloy composition of Ni/(Ir+Ni) <sup>b</sup> /%	Particle size of Ni-Ir alloy <sup>b</sup> /nm
0	H <sub>2</sub> 773 K, 1 h	24	3.2
1	Air, 723 K, 1 h + H <sub>2</sub> 773 K, 1 h	24	3.2
2	Air, 723 K, 1 h + H <sub>2</sub> 773 K, 1 h	21	3.8
4	Air, 723 K, 1 h + H <sub>2</sub> 773 K, 1 h	14	4.0

<sup>a</sup>Reaction conditions: catalyst 0.1 g, pyridine 5 mmol, methanol 3 g, H<sub>2</sub> 8 MPa, 353 K, 2 h.

<sup>b</sup>Determined by XRD analyses based on Vegard's law.

**Table S6** Summary of characterization of catalysts

Entry	Catalyst	Reduction temp. /K	Alloy composition <sup>a</sup> of Ni/(Ni+Ir) in Ni-Ir alloy /%	Metal dispersion <sup>b</sup> ( $H_{\text{total}}/(Ni+Ir)_{\text{total}}$ ) /%	TOF <sup>c</sup> /min <sup>-1</sup>	TOF <sub>s</sub> <sup>c</sup> /min <sup>-1</sup>
1	Ir/SiO <sub>2</sub>	773	0 <sup>d</sup>	22.0 <sup>d</sup>	2.6	12
2	Ni-Ir/SiO <sub>2</sub> -0.03	773	1 <sup>d</sup>	17.9 <sup>d</sup>	0.34	1.8
3	Ni-Ir/SiO <sub>2</sub> -0.05	773	2 <sup>d</sup>	16.9 <sup>d</sup>	0.22	1.2
4	Ni-Ir/SiO <sub>2</sub> -0.1	773	5 <sup>d</sup>	17.2 <sup>d</sup>	0.46	2.4
5	Ni-Ir/SiO <sub>2</sub> -0.15	773	6 <sup>f</sup>	14.4 <sup>g</sup>	0.29	20
6	Ni-Ir/SiO <sub>2</sub> -0.2	773	7 <sup>f</sup>	13.1 <sup>g</sup>	9.6	69
7	Ni-Ir/SiO <sub>2</sub> -0.25	773	8 <sup>d</sup>	12.0 <sup>d</sup>	11	97
8	Ni-Ir/SiO <sub>2</sub> -0.5	773	16 <sup>d</sup>	11.0 <sup>d</sup>	24	220
9	Ni-Ir/SiO <sub>2</sub> -1	773	24 <sup>d</sup>	9.5 <sup>d</sup>	22	231
10	Ni-Ir/SiO <sub>2</sub> -1(1073 K) <sup>e</sup>	1073	29 <sup>d</sup>	9.6 <sup>d</sup>	4.7	49
11	Ni-Ir/SiO <sub>2</sub> -1(1173 K) <sup>e</sup>	1173	39 <sup>d</sup>	6.1 <sup>d</sup>	0.59	9.6
12	Ni/SiO <sub>2</sub> (Ni=1.2 wt%)	773	100 <sup>d</sup>	9.7 <sup>d</sup>	<0.01	<0.01

<sup>a</sup>Determined by XRD analyses based on Vegard's law

<sup>b</sup>Estimated by H<sub>2</sub> adsorption.

<sup>c</sup>The details are shown in Table S7.

<sup>d</sup>The data are taken from [S1]

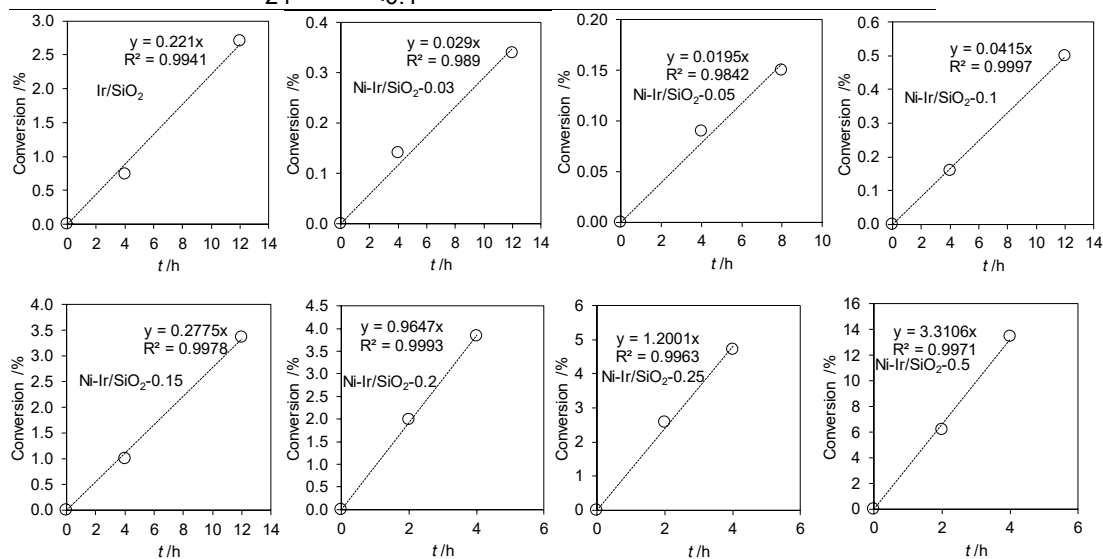
<sup>e</sup>The number in the parentheses is catalyst pre-reduction temperature.

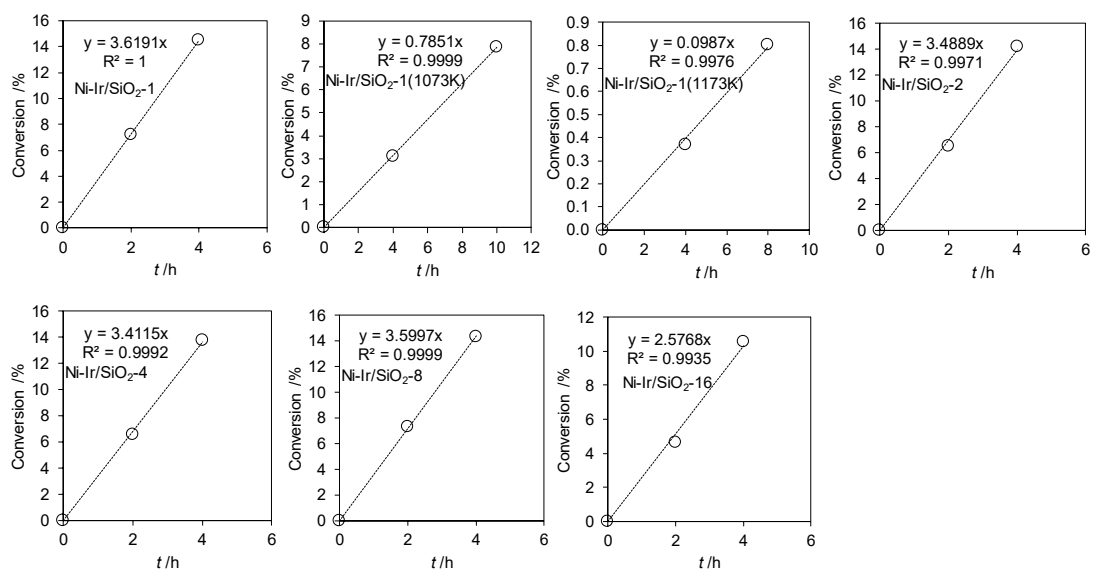
<sup>f</sup>The details are shown in Figure S1.

<sup>g</sup>The details are shown in Table S8.

**Table S7** Effect of Ni loading amount in hydrogenation of pyridine and the detailed time-course for calculation of TOF and TOF<sub>s</sub><sup>a</sup>

Catalyst	t/h	Conversion /%	Selectivity /%	TOF /min <sup>-1</sup>	TOF <sub>s</sub> /min <sup>-1</sup>
Ir/SiO <sub>2</sub>	0	0	-		
	4	0.74	>99.9	0.044	0.20
	12	2.70	>99.9		
Ni-Ir/SiO <sub>2</sub> -0.03	0	0	-		
	4	0.14	>99.9	0.0056	0.03
	12	0.34	>99.9		
Ni-Ir/SiO <sub>2</sub> -0.05	0	0	-		
	4	0.09	>99.9	0.0037	0.02
	8	0.15	>99.9		
Ni-Ir/SiO <sub>2</sub> -0.1	0	0	-		
	4	0.16	>99.9	0.0076	0.04
	12	0.5	>99.9		
Ni-Ir/SiO <sub>2</sub> -0.15	0	0	-		
	4	1.0	>99.9	0.048	0.34
	12	3.4	>99.9		
Ni-Ir/SiO <sub>2</sub> -0.2	0	0	-		
	2	2.0	>99.9	0.16	1.15
	4	3.8	>99.9		
Ni-Ir/SiO <sub>2</sub> -0.25	0	0	-		
	2	2.6	>99.9	0.19	1.61
	4	4.7	>99.9		
Ni-Ir/SiO <sub>2</sub> -0.5	0	0	-		
	2	6.2	>99.9	0.40	3.67
	4	13.5	>99.9		
Ni-Ir/SiO <sub>2</sub> -1	0	0	-		
	2	7.2	>99.9	0.36	3.82
	4	14.5	>99.9		
Ni-Ir/SiO <sub>2</sub> -1 (1073 K) <sup>b</sup>	0	0	-		
	4	3.1	>99.9	0.079	0.82
	10	7.9	>99.9		
Ni-Ir/SiO <sub>2</sub> -1 (1173 K) <sup>b</sup>	0	0	-		
	4	0.37	>99.9	0.0099	0.16
	8	0.8	>99.9		
Ni/SiO <sub>2</sub> Ni=1.2 wt%	2	<0.1	-		
	4	<0.1	-		
	24	<0.1	-		





<sup>a</sup>Reaction conditions: catalyst 0.02 g, pyridine 5 mmol, methanol 3 g, H<sub>2</sub> 8 MPa, stirring speed 500 rpm, 353 K.

<sup>b</sup>The number in the parentheses is catalyst pre-reduction temperature.

**Table S8** H<sub>2</sub> adsorption experiment with Ni-Ir/SiO<sub>2</sub>-0.15 and Ni-Ir/SiO<sub>2</sub>-0.2

Catalyst	Amount /g	Ni+Ir /mmol g <sup>-1</sup>	H <sub>total</sub> /mmol g <sup>-1</sup>	Dispersion (H <sub>total</sub> /(Ni+Ir)) /%
Ni-Ir/SiO <sub>2</sub> -0.15	0.104	0.239	0.0343	14.4
Ni-Ir/SiO <sub>2</sub> -0.2	0.100	0.249	0.0327	13.1

## References

- [S1] J.-q. Bai, M. Tamura, Y. Nakagawa and K. Tomishige, *Chem. Commun.*, 2019, **55**, 10519.
- [S2] J.-q. Bai, M. Tamura, A. Nakayama, Y. Nakagawa and K. Tomishige, *ACS Catal.*, 2021, **11**, 3293.
- [S3] J. W. Cook and D. E. Sayers, *J. Appl. Phys.*, 1981, **52**, 5024.
- [S4] K. Okumura, J. Amano, N. Yasunobu and M. Niwa, *J. Phys. Chem. B*, 2000, **104**, 1050.
- [S5] K. Okumura, S. Matsumoto, N. Nishiaki and M. Niwa, *Appl. Catal., B*, 2003, **40**, 151.
- [S6] A. L. Ankudinov, B. Ravel, J. J. Rehr and S. D. Conradson, *Phys. Rev. B*, 1998, **58**, 7565.
- [S7] V. Mévellec and A. Roucoux, *Inorg. Chem. Acta*, 2004, **357**, 3099-3103.
- [S8] M. Fang, N. Machalaba and R. A. Sánchez-Delgado, *Dalton Trans.*, 2011, **40**, 10621.
- [S9] M. Fang and R. A. Sánchez-Delgado, *J. Catal.*, 2014, **311**, 357-368.
- [S10] A. Sánchez, M. Fang, A. Ahmed and R. A. Sánchez-Delgado, *Appl. Catal. A*, 2014, **477**, 117-124.
- [S11] A. Karakulina, A. Gopakumar, i. Akçok, B. L. Roulier, T. LaGrange, S. A. Katsyuba, S. Das and P. J. Dyson, *Angew. Chem. Int. Ed.*, 2016, **55**, 292-296.
- [S12] F. Martinez-Espinar, P. Blondeau, P. Nolis, B. Chaudret, C. Claver, S. Castellón and C. Godard, *J. Catal.*, 2017, **354**, 113-127.
- [S13] F. Chen, W. Li, B. Sahoo, C. Kreyenschulte, G. Agostini, H. Lund, K. Junge and M. Beller, *Angew. Chem. Int. Ed.*, 2018, **57**, 14488-14492.
- [S14] X. Feng, Y. Song, J. S. Chen, Z. Li, E. Y. Chen, M. Kaufmann, C. Wang and W. Lin, *Chem. Sci.*, 2019, **10**, 2193-2198.
- [S15] K. Murugesan, V. G. Chandrashekar, C. Kreyenschulte, M. Beller and R. V. Jagadeesh, *Angew. Chem. Int. Ed.*, 2020, **59**, 17408-17412.
- [S16] N. Tanaka and T. Usuki, *Eur. J. Org. Chem.*, 2020, **34**, 5514-5522
- [S17] D. Chandra, S. Saini, S. Bhattacharya, A. Bhaumik, K. Kamata and M. Hara, *ACS Appl. Mater. Interfaces*, 2020, **12**, 52668–52677.
- [S18] R. Kokane, Y. Corre, E. Kemnitz, M. K. Dongare, F. Agbossou-Niedercorn, C. Michon and S. B. Umbarkar, *New J. Chem.*, 2021, **45**, 19572-19583.
- [S19] N. Antil, A. Kumar, N. Akhtar, W. Begum, M. Chauhan, R. Newar, M. S. Rawat and K. Manna, *Inorg. Chem.*, 2022, **61**, 1031-1040.
- [S20] M. Campanati, A. Vaccari and O. Piccolo, *J. Mol. Catal. A*, 2002, **179**, 287-292.
- [S21] H. Mao, C. Chen, X. Liao and B. Shi, *J. Mol. Catal.*, 2011, **341**, 51-56.
- [S22] D. Ren, L. He, L. Yu, R.-S. Ding, Y.-M. Liu, Y. Cao, H.-Y. He and K.-N. Fan, *J. Am.*

*Chem. Soc.*, 2012, **134**, 17592-17598.

[S23] R. Rahi, M. Fang, A. Ahmed and R. A. Sánchez-Delgado, *Dalton Trans.*, 2012, **41**, 14490-14497.

[S24] X. Xue, M. Zeng and Y. Wang, *Appl. Catal. A*, 2018, **560**, 37-41.

[S25] C. Liu, Z. Rong, Z. Sun, Y. Wang, W. Du, Y. Wang and L. Lu, *RSC Adv.*, 2013, **3**, 23984-23988.

[S26] H.-yan Jiang, Si-shi Zhang and B. Sun, *Catal. Lett.*, 2018, **148**, 1336-1344.

[S27] C. Ciotonea, N. Hammi, J. Dhainaut, M. Marinova, A. Ungureanu, A. E. Kadib, C. Michon and S. Royer, *ChemCatChem*, 2020, **12**, 4652-4663.